Romanian Reports in Physics, Vol. 59, No. 3, P. 805–817, 2007

TRIPLE – BARRIER RESONANT TUNNELING: A TRANSFER MATRIX APPROACH

CRISTIAN E. SIMION[1], CRISTIAN I. CIUCU[2]

[1]*NIPNE – National Institute of Materials Physics, Magurele, Romania*
[2]*University of Bucharest, Faculty of Physics, Magurele, Romania*

(Received October 14, 2006)

Abstract. A theoretical study of resonant tunneling in multilayered heterostructures is presented based on an exact solution of the Schrödinger equation under the application of a constant electric field and a uniform magnetic field. By use of the transfer matrix approach, the transmissivity of the structure is determined as a function of the incident electron energy. The results show good agreement with other existing models as well as with the bound-state energies. The solutions obtained are exact and can be generated easily by using MathCad. Based on these calculations, a new class of resonant tunneling superlattice devices can be designed.

Key words: resonant tunneling, AlGaAs/GaAs TBRT structures.

1. INTRODUCTION

Advanced crystal growth techniques, such as metal - organic vapor phase epitaxy (MOVPE) and molecular beam epitaxy (MBE) make it possible to obtain quantum wells and superlattices with reproducible properties at the atomic scale.

By a further reduction in the dimensionality, new electronic properties are revealed in one-dimensional quantum wires [1] and zero-dimensional quantum dots (the ultimate quantum confinement structure) [2].

Most of the initial work on electron transport in small systems has dealt with metallic samples. More recently, increasing attention has been paid to semiconductor-insulator structures, which can now be fabricated and controlled on a very small scale. In the absence of impurities, the sample boundaries become the only source of electron scattering. The short wavelength of the Fermi electrons in metals validates the use of a semiclassical picture where the electron is reflected by the internal walls of the sample and moves ballistically between collisions. On the other hand, the electron wavelength in semiconductor quantum wires may be comparable to the size of the sample, and in particular to the effective width of the

wire. In this regime, one can view the electron motion as the propagation of a wave in a guide, and quantum wires may appropriately be called "electron waveguides". This notation has recently found clear experimental verification.

This material is organized as follows: Section 2 gives details of geometry and composition for the TBRT device. Section 3 outlines the theoretical approach. In Section 4 we present numerical results of the transmission probability and $|\Psi|^2$ for some special TBRT structure.

2. GEOMETRY AND COMPOSITION FOR THE TBRT DEVICE

The conduction-band energy diagram for a TBRT structure is shown in Fig. 1 (a,b). By simply eliminating the coupling barrier, a TBRT structure transforms into a double-barrier (DBRT) one. These structures consist of two heavily doped $n+$ GaAs layers emitter and collector (˜ 2×10^{17} cm^{-3}), undoped AlGaAs barriers (30Å,Y=0.6) and the undoped GaAs quantum well (QW) regions (45Å). The conduction band offset ? E_c, effective mass $m^*(z)$ and dielectric constant e(z) in each region of the DBRT or TBRT structure are determined as function of the aluminum concentration $Y(z)$, by the following approximations [3]:

$$? E_c(z)=0.75Y(z) \text{ eV} \quad \text{for } 0=Y(z)=0.45 \tag{1a}$$

$$? E_c(z)=0.75y(Z)+0.69[y(Z)-0.45]^2 \text{ eV} \quad \text{for } 0.45<Y(z)=1 \tag{1b}$$

$$m^*(z)/m_0-0.067+0.083Y(z) \quad \text{for } 0<Y(z)<1 \tag{1c}$$

$$e(z)/e_0=13.1-3.0Y(z) \quad \text{for } 0=Y(z)=1 \tag{1d}$$

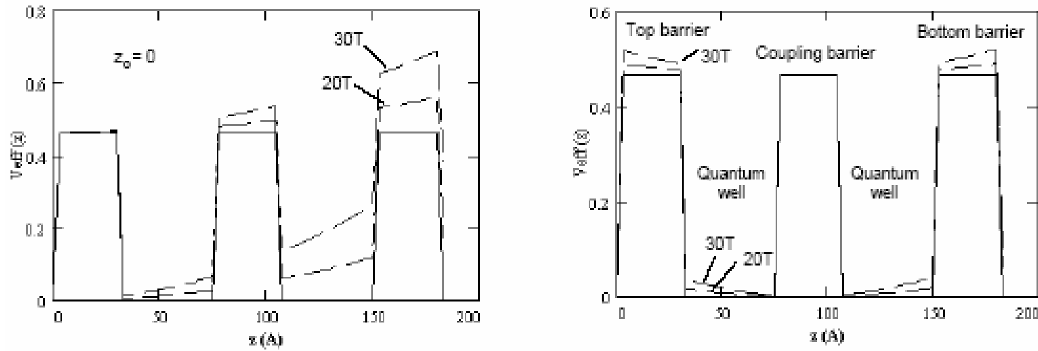

Fig. 1 – The effective one-dimensional potential $V(z)$ (in eV) as a function of transverse magnetic field B in a symmetric triple barrier resonant structure with $LB_1=LB_2=LB_3$=30Å, $YB_1=YB_2=YB_3$=0.6, $LQW_1=LQW_2$=45Å, for z_o=0 (a) and $z_o=L/2$ (b). The origin for z_o lies at the front of the top barrier and L stands for the total thickness of the TBRT structure.

3. THEORY

We assume for our resonant structures that the incoherent electron scattering, space-charge effects, many-electron effects and phonon-assisted tunneling are neglected. However, it should be noted that the interaction with phonons might be responsible for the satellite peaks in DBRT current, at voltages just above the resonant peak [4, 5].

Using the effective-mass single electron approximation, we then separate the three-dimensional single-electron Schrödinger equation into parts which are transverse and parallel to the device layers. The total electron energy E_{tot} is then written as the sum of these parallel and transverse components:

$$E_{tot} = \frac{E + \hbar^2 \left| k_{II} \right|^2}{2 \ m^*}, \tag{2}$$

where $\left| k_{II} \right|$ is the wave vector in the *x*-*y* plane parallel to the $Al_yGa_{1-y}As/GaAs$ interfaces. *E* is the electron kinetic energy perpendicular to the interfaces (i.e. in the *z* direction).

The total wave function can be expressed as a product:

$$\Psi(x, y, z) = \frac{1}{\sqrt{A}} e^{i \, k_{II} \cdot r_{II}} \varphi \ (z) \, . \tag{3}$$

A represents the device area k_{II} and r_{II} are vectors in the *x*-*y* direction, and $\boldsymbol{j}$ is the solution to the following one-dimensional Schrödinger equation:

$$-\frac{\hbar^2}{2} \frac{\mathrm{d}}{\mathrm{d}z} \left(\frac{1}{m^*(z)} \right) \frac{\mathrm{d}\varphi}{\mathrm{d}z} + U(z) \boldsymbol{j} \ = E \boldsymbol{j} \, . \tag{4}$$

In this relation $m^*(z)$ denotes the position-dependent electron (band gap) effective mass and $U(z)$ is the potential seen by a single electron, which includes effects of both conduction-band discontinuities at $Al_xGa_{1-x}As/GaAs$ interfaces and external applied voltage. This model can be seen in Fig. 2.

To solve for the transmission probability, we use a transfer–matrix method similar to the one presented, for example, by Ando and Itoh [6]. This method, in which the exact potential is approximated by a series of steps (details can be seen in Fig.2), has among its advantages computational simplicity and good accuracy.

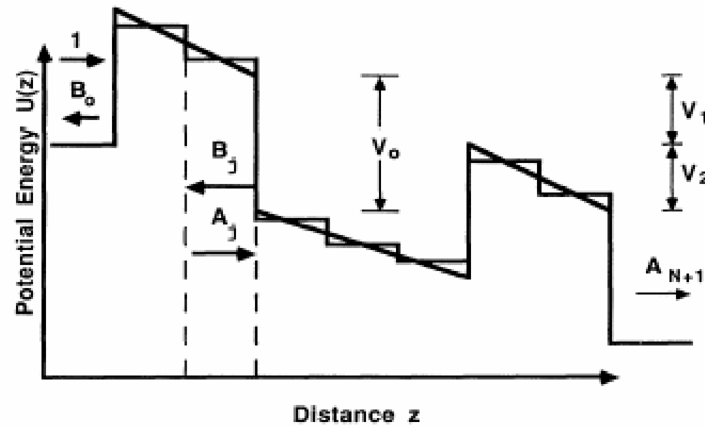

Fig. 2 – Schematic drawing of the exact potential $U(z)$ for a double-barrier structure and the step approximation used in transfer matrix calculations. Device has parameters d_1=60Å, d_2=30Å, and V_0=684meV.

The main problem is quit simple, if we treat the potential as constant over each step. In this case the solution to the one-dimensional Schrödinger equation is given in the jth step as a superposition of plane waves:

$$\varphi_j(z_j) = A_j e^{k_j z_j} + B_j e^{-k_j z_j} \tag{5}$$

and we have the z component of the complex wave vector K_j given by:

$$K_j = \left[\frac{2m_j^*(U_j - E)}{\hbar^2}\right]^{1/2} \tag{6}$$

and $j = 0,1,2,\ldots,N, N+1$ for a total of $N+1$ steps. Here U_j and m^*_j are the potential and effective mass associated with step j, and z_j is distance measured from the left-hand side of the jth step. Furthermore, the steps are all assumed to have the same length a and j values increase as the structure is traversed from left to right (see arrows in Fig. 2).

Imposing continuity of the wave function φ and its appropriately normalized derivative $(1/m^*)(\mathrm{d}\boldsymbol{j}\ /\mathrm{d}z)$ at the boundary between steps j and $j+1$, one derives a matrix formula that relates the successive A and B plane-wave coefficients, namely

$$\begin{bmatrix} A_{j+1} \\ B_{j+1} \end{bmatrix} = M_j \begin{bmatrix} A_j \\ B_j \end{bmatrix}, \tag{7}$$

where

$$M_j = \frac{1}{2}\begin{bmatrix} (1+\rho_j)\exp(k_j a) & (1-\rho_j)\exp(-k_j a) \\ (1-\rho_j)\exp(k_j a) & (1+\rho_j)\exp(-k_j a) \end{bmatrix}, \quad (8)$$

for

$$\rho_j = \frac{m^*_{j+1} k_j}{m^*_j k_{j+1}}. \quad (9)$$

At this moment the M_j matrices are then multiplied together to relate the plane-wave coefficients A_0 and B_0 in the emitter layer to the coefficients A_{N+1} and B_{N+1} in the collector layer:

$$\begin{bmatrix} A_{N+1} \\ B_{N+1} \end{bmatrix} = M_{tot} \begin{bmatrix} A_0 \\ B_0 \end{bmatrix}, \quad (10)$$

with

$$M_{tot} \equiv \begin{bmatrix} M_{11} & M_{12} \\ M_{21} & M_{22} \end{bmatrix} = M_N \ldots M_1 M_0. \quad (11)$$

If we use the relation $\det(M_j)=\boldsymbol{r}_j$, which in turn leads to $\det(M_{tot})=k_0/ k_{N+1}$ and setting $A_0=1$ and $B_0=0$ in Eq. (10) corresponding to an electron incident form the left-hand side of Fig.2 we find a simple formula for the transmission amplitude A_{N+1}.

$$A_{N+1} \frac{k_0}{k_{N+1}} \left[\frac{1}{M_{22}} \right]. \quad (12)$$

Note that the effective-mass factors cancel because the collector and emitter layers have identical material composition.

Now the transmission probability T can be write as the ratio of transmitted particle flux and depends on both the incident electron energy E and the applied voltage V.

$$T(E,V) = \frac{|k_{N+1}|}{|k_0|} |A_{N+1}|^2. \quad (13)$$

Once the transmitted wave amplitude A_{N+1} is found from the Eq.(12), the left electronic wave function can be calculated across the entire structure by inverting the M_j and then successively solving for the A_j and B_j according to:

$$\begin{bmatrix} A_j \\ B_j \end{bmatrix} = M_j^{-1} \begin{bmatrix} A_{j+1} \\ B_{j+1} \end{bmatrix}, \quad (14)$$

where

$$M_j^{-1}=\frac{1}{2}\begin{bmatrix}(1+1/\rho_j)\exp(-k_j a) & (1-1/\rho_j)\exp(k_j a)\\ (1-1/\rho_j)\exp(k_j-a) & (1+1/\rho_j)\exp(k_j a)\end{bmatrix}. \tag{15}$$

Once the transmission probability is obtained, the current density through the structure is calculated using the Tsu-Esaki current formula [7].

$$J=\frac{em^* k_b T}{2\pi^2\hbar^3}\times\int_0^\infty T(E;V)\ln\left[\frac{1+\exp(E_F-E)/k_bT}{1+\exp(E_F-E-eV)/k_bT}\right]\mathrm{d}E\,, \tag{16}$$

where E_F is the Fermi energy, T is the temperature, E is the electron kinetic energy transverse to the device layers, k_b is the Boltzmann constant, and m^* is the electron effective mass in GaAs.

We assume a constant magnetic field in the x-direction $\boldsymbol{B}=(B,0,0)$. This can be represented by a vector potential in the gauge $\boldsymbol{A}=(0,-Bz,0)$. Then the following Hamiltonian describes a spinless particle in a layer of the structure, with an effective mass $m^*(z)$ and charge $-e$, subject to a constant and uniform transverse magnetic field $\boldsymbol{B}$:

$$H=-\frac{\hbar^2}{2m^*}\Delta-ie\frac{\hbar}{m^*}A\cdot\vec{\nabla}+\frac{e^2A^2}{2m^*}+V(z), \tag{17}$$

where $V(z)$ is the potential-energy seen by a single electron, which includes effects of both conduction-band discontinuities at GaAs/Al_yGa_{1-y} interfaces and external applied bias. The incoherent electron scattering, space-charge effects, many-electron effects and phonon-assisted tunneling are neglected. However, it should be noted that the interaction with phonons may be responsible for the satellite peaks in DBRT current, at voltages just above the resonant peak [8]. The stationary Schrödinger equation corresponding to the Hamiltonian (17) is therefore. Notice that the choice of vector potential is not unique for the given magnetic field. With a different one the solutions would then look very different while the physics must remain the same. It is only with our choice of gauge, that the solutions have translation symmetry in the x and y directions. Therefore the wave function ?(r) can be written as a product of a plane wave with an anvelope wavefunction f (z) describing the motion of the tunneling electrons along the z-direction of the structure $\boldsymbol{y}(r)=\boldsymbol{j}(z)\exp\left[\mathrm{i}\left(K_x x+K_y y\right)\right]$. By substituting this wave function into the stationary Schrödinger's equation we obtain a basically one-dimensional Schrödinger equation for the anvelope wavefunction f (z):

$$\frac{\mathrm{d}^2\varphi}{\mathrm{d}z^2}+\frac{2m^*}{\hbar^2}\left\{\left(E-\frac{\hbar^2k_x^2}{2m^*}\right)-\left[V(z)+\frac{e^2B^2}{2m^*}\left(z-z_0\right)\right]\right\}\varphi=0\,. \tag{18}$$

We note that the influence of the magnetic field is included by changing the ordinary superlattice potential and external applied bias effects *V(z)*, with an effective one dimensional potential V_{eff} :

$$V_{eff} = V(z) + \frac{1}{2} m^*(z) \;\; \omega_c^2(z) \;\; (z - z_0)^2, \tag{19}$$

where $z_0 = l_B^2 K_{y0}$, with the magnetic length, and ? $_c(z)$ stands for the cyclotron frequency associated with a z-dependent effective mass $m^*(z)$. The parameter z_o gives the center of the cyclotron orbit. Due to ionized impurity scattering, the coherence of the Landau motion is destroyed in emitter and collector regions. Hence it is expected that the effect of the magnetic field in these regions be small enough to set for the magnetic vector potential $\boldsymbol{A}_{emitter} = \boldsymbol{A}_{collector}$ ˜ 0. We used a transfer-matrix (TM) method [9] to solve this one-dimensional Schrödinger equation and to calculate the transmission probability, resonant line widths, the transit time and the anvelope wavefunctions f (z) for the motion along z-axis, under or without applied bias V_a and magnetic field $\boldsymbol{B}$, perpendicular to z-axis.

This method has been widely used due to its simplicity related with the use of only 2×2 matrices and with the possibility of studying superlattices formed by *any sequences oflayers*. We discretize the barrier and the quantum-well (QW) regions into a finite number of steps, so that, at any step, a flat-band potential approximation can be used.

Ando and Itoh [6] have shown that as the number of steps increases and the new step-like potential will be closer and closer to $V_{eff}(z)$, the solution rapidly converges to a single result. Therefore, at any step, the solution to the Schrödinger equation (18) is given as a superposition of waves $\varphi(z) = a \cdot \exp(K_z z) + b \cdot \exp(-K_z z)$? with the z component of the wave vector K_z given by:

$$K_z(z) = \sqrt{\frac{2m(z)^*}{\hbar^2}\left\{\left[V(z) + \frac{e^2B^2}{2m(z)^*}(z - z_0)^2\right] - \left(E - \frac{m_0^*}{m(z)^*}E_{x,0}\right)\right\}}, \tag{20}$$

where m_0^* and $E_{x,0}$ are the effective mass and the kinetic energy along x axis, in the emitter region. Using a boundary condition that conserves carrier current (the continuity of the anvelope wavefunction f (z), and its first derivative divided by $m^*(z)$,f (z)'/m^*), the coefficients a_j and b_j of region j are joined to those of region $j+1$ by a 2×2 transfer matrix $\boldsymbol{T}_{j,j+1}$ of determinant 1:

$$\begin{pmatrix} a_{j+1} \\ b_{j+1} \end{pmatrix} = T_{j,j+1} \begin{pmatrix} a_j \\ b_j \end{pmatrix}. \tag{21}$$

4. TRIPLE BARRIER RESONANT STRUCTURE

In this section we study how energy level of the coupling barrier influence the transmission probability coefficient. Also we present numerical results showing the influence of coupling barrier thickness, and position of it in the quantum well on transmission probability and coupling energy.

4.1. THE INFLUENCE OF THE COUPLING BARRIER ENERGY ON TRANSMISSION PROBABILITY FOR A GaAs/AlYGa$_{1-Y}$As (TBRT) DEVICE

We consider a symmetric triple-barrier resonant tunneling device (TBRT), with same aluminum concentration in lateral AlGaAs barriers $x_{B1}=x_{B5}=0.6$ (that means $m_2^*=0.1168m_0$, and $V_0=0.465525$eV).

For the quantum well GaAs regions we use $m_1^*=0.067m_0$, $V_0=0$ eV. For the coupling barrier energy we will use three different aluminum concentration values.

Sharp peaks occur in the transmission for the resonant energies E_{01}, E_{02} and E_{11}, E_{12} (Fig. 3). These are the energies corresponding to the ground quasibound doublet and the first excited one. Increasing the coupling barrier aluminum concentration the transmission peaks shift higher in energy. It should be noted that the coupling energy for the ground quasibound doublet has a different increase than the excited one.

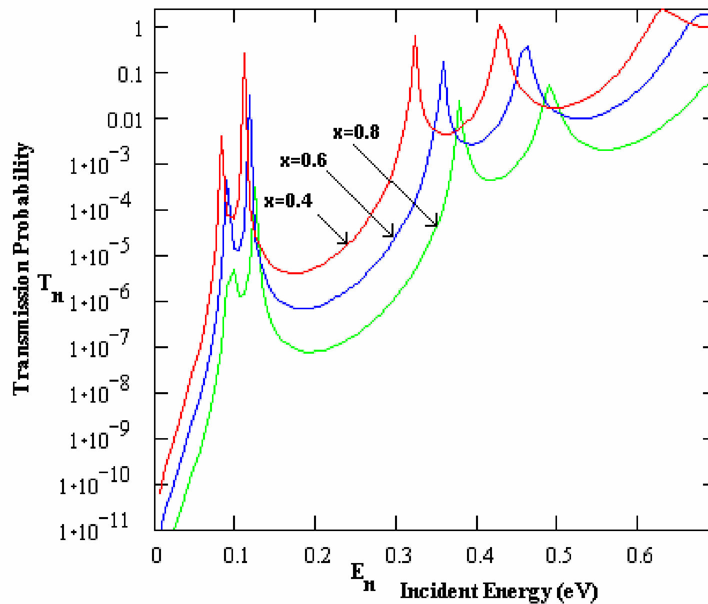

Fig. 3 – Transmission probability *versus* incident energy for TBRT with different coupling barrier energy.

These doublets are generated by splitting the symmetric ground states and the antisymmetric excited ones of an isolated quantum well into a symmetric-antisymmetric pair.

The symmetric states have, as expected, lower energy. Such a splitting is caused by the coupling between the wells (this means that the degeneracy of each level is removed due to a coupling barrier of finite thickness). Also, each resonant level has a finite width induced by the coupling with the left (emitter) and right (collector) justified states in the continuum spectrum.

Figure 3 shows a plot of the transmission probability *vs*. incident energy for a TBRT for different aluminum concentration values.

4.2. THE INFLUENCE OF THE THICKNESS COUPLING BARRIER ON TRANSMISSION PROBABILITY FOR A GaAs/AlYGa$_{1-Y}$As (TBRT) DEVICE

Our triple-barrier resonant structure (TBRT) has $d_{B1}= d_{B5}$=30A, $d_{G2}=d_{G4}$=60A, $x_{B1}=x_{B5}=x_{B3}$=0.67, $x_{B2}=x_{B4}$=0, but the coupling barrier has a different thickness. For this time Al molar fraction of the central barrier is y_{B4}=0.67 (has the same height as first and last barrier).

We observe that the first resonant doublet has a specific behavior for different values of the central barrier. The first resonant level $E^{(1,1)}$ slowly decease from 0.161805meV for d_{B4}=50Å, to 0.12687meV for d_{B4}=10Å, about 22% from the initial value. Meanwhile the second resonant doublet increasing with 44meV from 0.163353eV for d_{B4}=50Å up to 0.207715eV for d_{B4}=10Å. That means about 27% from the initial value. The ground quasibound doublet splitting more and more with central barrier thickness less.

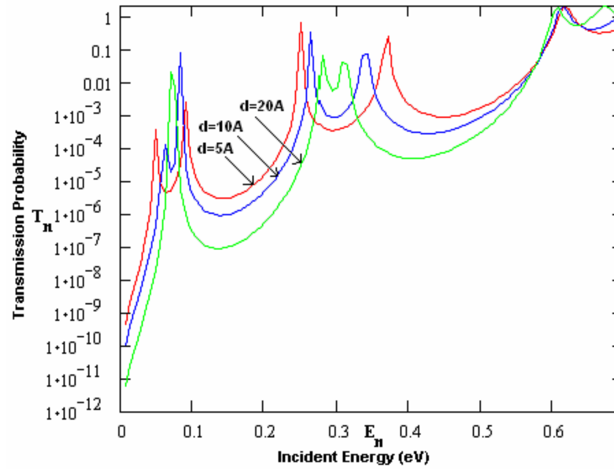

Fig. 4 – Transmission probability *versus* incident energy for TBRT with different thickness of coupling barrier.

4.3. TRANSMISSION PROBABILITY FOR TBRT WITH APPLIED BIAS

For numerical simulation we use a TBRT with the same thickness of the lateral barriers as the central barrier (symmetric structure). $LB_1=LB_2=LB_3$=30A, $YB_1=YB_2=YB_3$=0.6 (m_1^*=0.067m_0, m_2^*=0.09439m_0), $LQW_1=LQW_2$=45A.

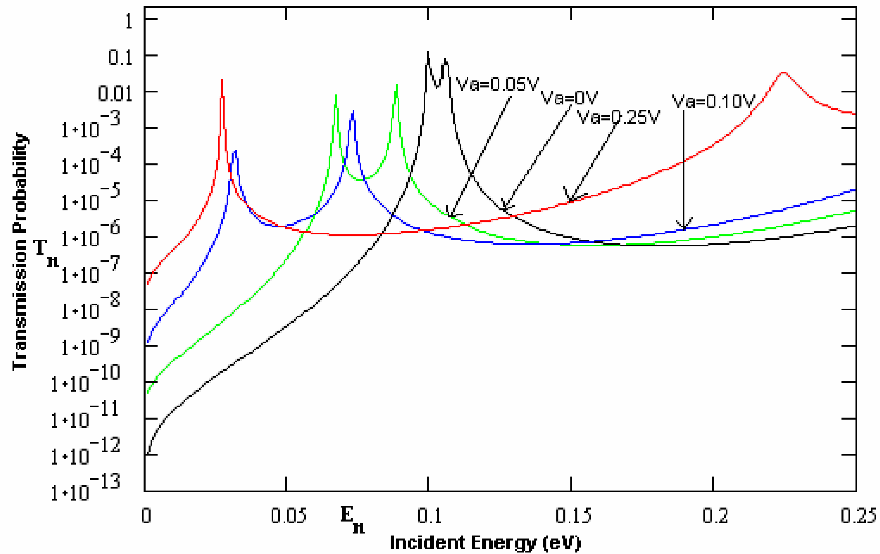

Fig. 5 – The effect of an applied bias on the transmission probability for the first resonant doublet of the TBRT.

For the values of applied bias less then V_0 an maximum for the transmission coefficient can be seen.

As we increase the applied bias the transmission probability spectrum slowly decease down to small electron energy values.

4.4. TRANSMISSION PROBABILITY AND COUPLING ENERGY *VS.* MAGNETIC INDUCTION

We have plotted in Fig. 6(a, b) the effect of an increasing transverse magnetic field ***B*** on the transmission probability, for the first and the second resonant doublet, respectively. The TBRT structure is the same as in Fig. 1, with zero applied bias and z_o=0. In this case, for *B*?0, the effective potential is no longer symmetric and therefore the transmission probability no longer achieves a peak value of 1.

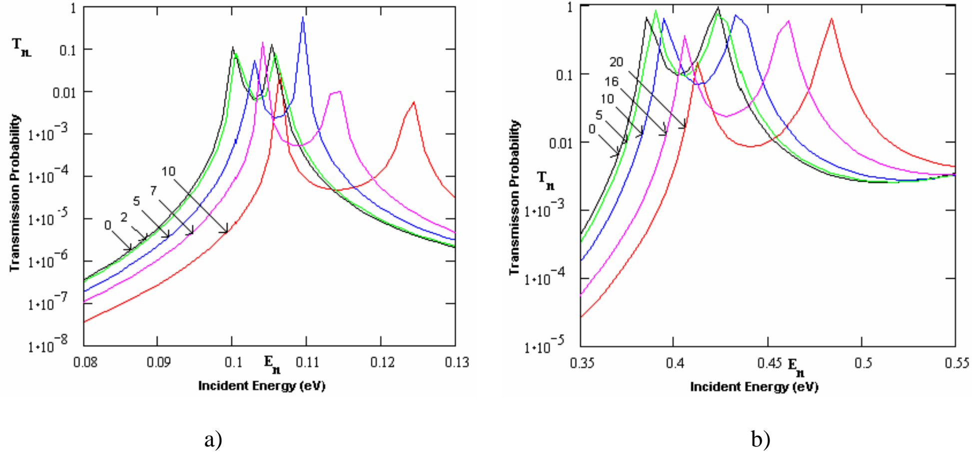

a) b)

Fig. 6 – The effect of an increasing transverse magnetic field on the transmission probability, for the first (a), and the second (b) doublet. The TBRT device with no applied bias and z_o=0. Numbered arrows indicate the magnetic induction in units of Tesla.

Sharp peaks occur in the transmission for the resonant energies E_{01}, E_{02} (Fig. 6a) and E_{11}, E_{12} (Fig. 6b). These are the energies corresponding to the ground quasibound doublet and the first excited one. Increasing the magnetic field the transmission peaks shift higher in energy. This is reasonable because the magnetic contribution to V_{eff} is, somehow, equivalent to a reverse bias applied on the structure. Figure 7(a, b) show a plot of the resonant lines *versus* magnetic induction B, for the first and second doublet, respectively. The results presented show that the splitting between the resonant lines (and hence the coupling energy *vs.* B), for each resonant doublet, also shifts up in energy by increasing the magnetic induction. It should be noted that the coupling energy for the ground quasibound doublet is much more affected by the magnetic field than the excited one. These doublets are generated by splitting the symmetric ground states and the antisymmetric excited ones of an isolated quantum well into a symmetric-antisymmetric pair. The symmetric states have, as expected, lower energy. Such a splitting is caused by the coupling between the wells (this means that the degeneracy of each level is removed due to a coupling barrier of finite thickness). Also, each resonant level has a finite width induced by the coupling with the left (emitter) and right (collector) justified states in the continuum spectrum. Note that, by increasing the thick nesses of the top and bottom barriers, the results are rapidly converging to those describing an isolated system with two coupled quantum-wells or an isolated quantum well (when the coupling barrier is removed).

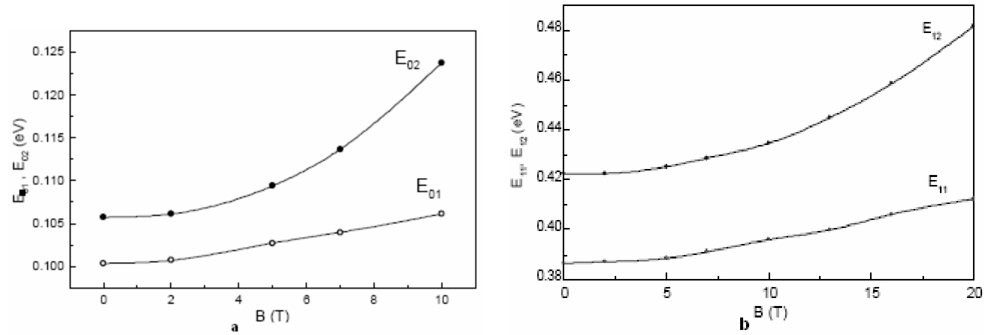

Fig. 7 – Resonant lines *versus* magnetic induction, for the ground doublet (a) and the excited doublet (b) z_o=0, without applied bias.

5. CONCLUSIONS

In this letter we have numerically examined the transmission probability and electronic wave functions in GaAs/Al_yGa_{1-y}As triple-barrier structures.

The sensitivity of spatial properties of electronic wave functions on DBRT device parameters suggests the possibility of "wave-function engineering". Thus, for example, the width of the well and the height of the barriers might be experimentally designed in order to minimize the effect of electron-confined-LO-phonon coupling, or to enhance scattering via one phonon mode over another. The effects of band nonparabolicity may also become important if the electrons are sufficiently "hot". While there are sophisticated ways of treating such effects, the simplest method is to define an energy-dependent effective mass [10]. This has been found to give good agreement between theory and experiment and we note that such an energy-dependent effective mass can be easily incorporated into our transfer-matrix calculation. Finally, we note that other complex effects such as many-electron interaction, interface scattering, can be important in certain real devices [11]. The possible role of such effects in experimental measurements depends sensitively on device parameters and should be considered in constructing a complete picture of resonant tunneling in double and triple barrier resonant structures.

REFERENCES

1. 1. J.P. Colinge, X. Baie, V. Bayot and E. Grivei, Solid-St. Electron., **39**, 49 (1996).
2. H. Drexler *et al.*, Phys. Rev. Lett., **73**, 2252 (1994).
3. H. C. Casey and M. B. Panish, *Heterostructure Lasers*, Academic, New York, 1978.
4. V. J. Goldman, D.C. Tsui, and J. E. Cunningham, Phys. Rev., B **36**, 7635 (1987).

5. M. L. Leadbeater, E. S. Alves, L. Eaves, M. Henini, O. H. Hughes, A. Celeste, J. C. Portal, G. Hill, and M. A. Pate, Phys. Rev., B **39**, 3438 (1989).
6. Y. Ando and T. Ytoh, J. Appl. Phys., **61**, 1497 (1987).
7. R. Tsu and L. Esaki, Appl.Phys.Lett., **22**, 562 (1973).
8. K.F. Brennan and C.J. Summers, *Theory of resonant tunneling in a variably spaced multiquantum well structure: An Airy function approach*, J.Appl.Phys., **61** *2*, 15 Jan 1987.
9. J.S. Walker, J. Gathright, *A transfer-matrix approach to one-dimensional quantum mechanics using Mathematica*®, Computer in physics, **6**, *4*, Jul/Aug (1992).
10. K.F. Brennan and C.J. Summers, J.Appl.Phys., **61**, *2*, 15 Jan. (1987).
11. M.O. Vassell, J. Lee, and H.F. Lockwood, J.Appl. Phys., **54**, 5206 (1983).